

## Quasi One-Dimensional Ionizing MPD Flow

G. Lefever-Button and V. V. Subramaniam  
 Department of Mechanical Engineering  
 The Ohio State University  
 Columbus, Ohio 43210  
 U.S.A.

### Abstract

Quasi one-dimensional models can serve as useful testbeds for testing various numerical algorithms for integrating the types of stiff differential equations that result from including finite rate kinetics (i.e. ionization and recombination). They are an important prelude to more complicated multi-dimensional simulations. In this paper, an earlier quasi one-dimensional model is extended to study the effects of varying area on *ionizing* MPD flow. Three popular numerical integrators of chemical rate equations (Runge-Kutta, Gear, and Bulirsch-Stoer) are compared for speed and accuracy. Based on the tests reported here, the Bulirsch-Stoer algorithm appears far superior. Results are also presented for MPD channel flow with area variation and finite rate kinetics. Comparisons of the thrust computed using the present quasi one-dimensional model with the recent experimentally measured values for the HSFAT (Half-Scale Flared Anode Thruster) are excellent. An important outcome of this work is the finding that channel divergence has significant effects not only on the thrust, but also on ionization and current density profiles.

### Nomenclature

<i>a</i>	Frozen speed of sound
<i>A</i>	Area
<i>B</i>	Magnetic induction
<i>e</i>	Electronic charge
<i>E</i>	Electric field
<i>h</i>	Enthalpy per unit mass
<i>j</i>	Current density
<i>J</i>	Total current

<i>k</i>	Boltzmann's constant
<i>k<sub>f</sub></i>	Ionization rate constant
<i>k<sub>r</sub></i>	Recombination rate constant
<i>l</i>	Computed channel length
<i>L</i>	Given channel length
<i>m<sub>A</sub></i>	Atomic mass
<i>ṁ</i>	Mass flow rate
<i>M</i>	Mach number
<i>P</i>	Pressure
<i>T</i>	Temperature
<i>u</i>	Velocity
<i>x</i>	Coordinate along channel
<i>α</i>	Ionization fraction
<i>ε<sub>i</sub></i>	Ionization potential of gas
<i>μ<sub>o</sub></i>	Permeability of free space
<i>ρ</i>	Mass density
<i>σ</i>	Electrical conductivity
*	superscript for quantities evaluated at the sonic point
<i>e</i>	subscript denoting exit values
<i>i</i>	superscript denoting <i>i</i> <sup>th</sup> iteration
<i>i</i>	subscript denoting inlet values

### I. Introduction

Earlier theoretical works have considered one-dimensional and quasi one-dimensional models of MPD flows (see for instance refs.[1]-[8]). The main motivation for such drastic simplifications has been to study the influence of individual phenomena on MPD flow, either as a prelude to studies of complicated multi-dimensional plasma

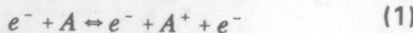
flows or to arrive at a basic understanding of operating limits and Onset phenomena. However, there exists another important use for these models. Quasi one-dimensional models that include finite rate kinetics can act as test beds for numerical algorithms that may be used in multi-dimensional simulations. Alternatively, simple models are often very effective design tools. It is with these goals in mind that we extend a previous one-dimensional flow model with finite rate kinetics[5], to include varying-area channels.

Finite rate kinetics introduce numerical stiffness that often overwhelms the speed and even stability of the best algorithms[9]. Further, quasi 1-D models, unlike multi-dimensional simulations, are complicated by the existence of singular points such as saddle points, nodes, and spirals (foci)[10]. In this paper, the back-EMF theory is extended to include the effects of area variation. Also, the best presently available numerical techniques for handling stiff systems are compared.

This paper is organized as follows. The model assumptions and governing equations are discussed next, followed by a discussion of the numerical procedures used to integrate these equations. The results for select cases are then discussed, followed finally by the summary and conclusions.

## II. Governing Equations

We consider here the equations of quasi 1-D, steady flow with the electric field perpendicular to the flow direction. The self-generated magnetic induction is taken to be perpendicular to both this electric field and the flow direction. This is tantamount to the assumption of negligible Hall effect. Further, we assume the MPD plasma to be composed of electrons, neutrals, and singly charged ions. Finite rate kinetics are included in the overall collisional reactions of electron-impact ionization and three-body recombination:



The ionization rate  $k_f$  and recombination rate  $k_r$ , for argon are[5]:

$$k_f = \frac{48 \times 10^{-9} \exp(-\varepsilon_i/kT)}{T^3 (5.556 \times 10^{-11})^{3/2}} \quad (cm^3/s) \quad (2)$$

$$k_r = 4 \times 10^{-9} T^{-9/2} \quad (cm^6/s)$$

where  $\varepsilon_i$  is the ionization potential of the propellant. The conservation equations are:

mass:

$$\frac{d}{dx}(\rho u A) = 0 \quad (3)$$

momentum:

$$\frac{dP}{dx} + \rho u \frac{du}{dx} + \frac{d}{dx}(B^2/2\mu_0) = 0 \quad (4)$$

energy:

$$\rho u \frac{dh}{dx} + \rho u^2 \frac{du}{dx} - Ej = 0 \quad (5)$$

state:

$$h = \frac{5P}{2\rho} + \frac{\varepsilon_i \alpha}{m_A} \quad (6)$$

rate:

$$\frac{d\alpha}{dx} = \frac{k_f \rho \alpha (1 - \alpha)}{m_A u} - \frac{k_r \rho^2 \alpha^3}{m_A^2 u} \quad (7)$$

Gauss' law:

$$\frac{d}{dx}(EA) = 0 \quad (8)$$

Ampere's law:

$$\frac{dB}{dx} = -\mu_0 j \quad (9)$$

Ohm's law:

$$j = \sigma(E - uB) \quad (10)$$

Although viscous and two-temperature effects are known to be important[11], they are neglected here. The existence of two distinct flow regimes, one dominated by ohmic heating

and the other by the electromagnetic body force, leads to the magnetogasdynamics sonic or choking condition [5]. This choking condition determines the electric field at the sonic point:

$$E^* = \frac{7}{4} a^* B^* + \{\beta_1 + \beta_2 + \beta_3\}^{1/2} \quad (11)$$

where  $\beta_1 = \frac{9}{16} a^* B^*^2$ ,

$$\beta_2 = \frac{5 P^* a^*}{2 \sigma^* A^*} \frac{dA}{dx} \Big|_{x=x^*}, \text{ and}$$

$$\beta_3 = \frac{\rho^* a^*}{\sigma^*} \frac{\varepsilon_i}{m_A} \frac{d\alpha}{dx} \Big|_{x=x^*},$$

and \* denotes quantities evaluated at the sonic point, i.e. where the flow speed equals the local frozen speed of sound[5]. This sonic or choking condition has been the subject of much confusion [12,13], but a rigorous treatment including proofs can be found in ref.[10].

### III. Numerical Procedure

Before proceeding with a discussion of the solution procedure of the system (3) through (10), we briefly describe three integrators of systems of ordinary differential equations. These integrators are (1) 4<sup>th</sup> order Runge-Kutta with variable step size, (2) Gear's predictor-corrector method[14], and (3) Bulirsch-Stoer extrapolation technique[15].

In the 4<sup>th</sup> order Runge-Kutta method, functional values at the initial point, two intermediate points, and a trial endpoint are used. Derivatives are then evaluated at each of these four points, and a weighted average of these values is used to calculate the end point value.

The Bulirsch-Stoer method uses rational function extrapolation (Richardson extrapolation) in order to extrapolate interim solutions to that corresponding to a zero step size. This is achieved by successively bisecting the original interval and subsequent subintervals, and integrating using the midpoint method (2<sup>nd</sup> order Runge-Kutta)[16]. In contrast to these two, Gear's method uses many initial and/or previous points to predict the functional value at the next point. A corrector equation specially formulated

for stiff equations is then used to iterate on the functional value at the next point.

Although all three numerical methods are capable of handling stiff equations, they vary considerably in the handling of the sonic singularity. Consequently, these techniques were first tested on the quasi 1-D isentropic flow equations of classical gas dynamics. This test isentropic flow problem consisted of an area variation given by  $A(x) = 1.98x^2 - 3.96x + 2$  ( $m^2$ ), channel length of 2 meters, upstream stagnation pressure of  $1.01 \times 10^6$  N/m<sup>2</sup>, upstream stagnation temperature of 273 K, and  $\rho_o = 1.7798759259$  Kg/m<sup>3</sup>. A comparison of the three numerical methods in terms of the number of right hand side evaluations, number of bisections to evaluate the correct inlet velocity, and total elapsed CPU time (run on a VAX 8500), is shown in Fig. 1. In Fig. 2, the overall accuracy of the three methods is compared. It can be seen that the best compromise between speed, efficiency, and accuracy, is the Bulirsch-Stoer algorithm. This is evident when all three methods are compared for speed while holding the total error constant to within the same order of magnitude. In this case, the Bulirsch-Stoer algorithm is seen to be most efficient, followed by the Gear method, and then by the 4<sup>th</sup> order Runge-Kutta method with variable step size.

The system (3) through (10) may be simplified since the density, electric field, and enthalpy may be computed directly from:

$$\rho u A = \text{constant} \quad (12)$$

$$EA = \text{constant} \quad (13)$$

$$h = \frac{5 P}{2 \rho} + \alpha \frac{\varepsilon_i}{m_A} \quad (14)$$

This leaves the following four equations to be integrated:

$$\frac{dB}{dx} = -\mu_o \sigma (E - uB) \quad (15)$$

$$\frac{d\alpha}{dx} = \frac{k_f \rho \alpha (1 - \alpha)}{m_A u} - \frac{k_r \rho^2 \alpha^3}{m_A^2 u} \quad (16)$$

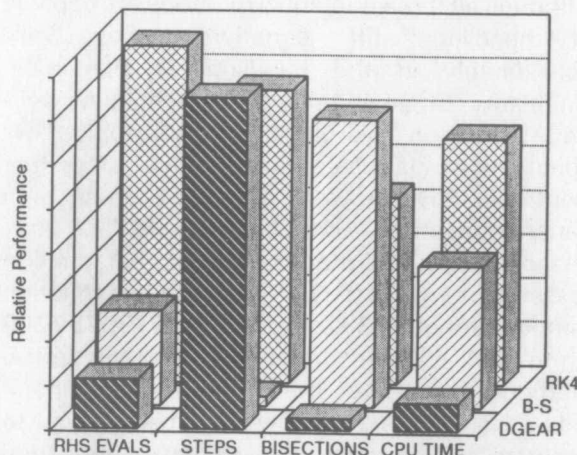


**Figure 1:** Comparison of integrator performance characteristics for isentropic test case.

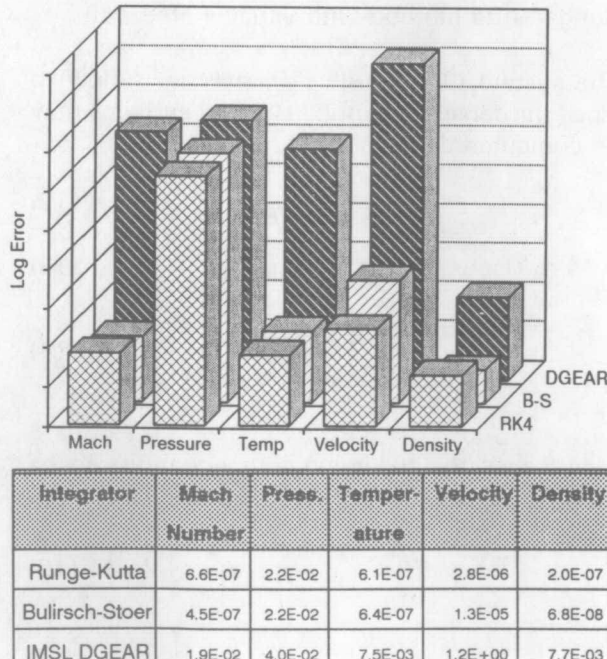


**Figure 2:** Comparison of overall integration errors for isentropic test case.

$$\frac{du}{dx} = \frac{\left\{ \frac{5}{3} \frac{P u}{\rho A} \frac{dA}{dx} + \frac{2}{3} u \frac{\varepsilon_i}{m_A} \frac{d\alpha}{dx} + \frac{5}{3} \frac{u}{\rho} B_j - \frac{2}{3\rho} E_j \right\}}{u^2 - a^2} \quad (17)$$

$$\frac{dP}{dx} = B\sigma(E - uB) - \rho u \frac{du}{dx} \quad (18)$$

The above system, along with the associated boundary conditions, constitutes a two-point boundary value problem. At the nozzle inlet, the mass flow rate and magnetic induction are known. The nozzle area variation as a function of position  $x$  is given, as is the total thruster length. The temperature, velocity, and ionization fraction at the inlet must be solved for, such that the downstream flow exiting the thruster is supersonic. The value of the electric field at the inlet must also be determined so that the sonic condition is satisfied. However, the location of the sonic point is not known a priori. **The correct inlet values can only be determined after the sonic point is successfully crossed.** Since the sonic point is a mathematical singularity, a "jump" algorithm is needed to cross it.

An iterative procedure is used to cross the sonic point. This proceeds as follows. Let the adjacent point on the subsonic side of the sonic point be denoted by the subscript 1, and the adjacent point on the supersonic side by the subscript 2. Let  $M_2 = 2 - M_1$ . The temperature at the pre-sonic point  $T_1$  is used as an initial approximation for  $T_2$ . Then  $u_2$  is computed from:

$$u_2^{(i)} = M_2 \left[ \frac{5}{3} \frac{k_B}{m_A} T_2^{(i-1)} (1 + \alpha_2^{(i-1)}) \right]^{1/2} \quad (19)$$

where the superscript  $i$  refers to the  $i^{\text{th}}$  iteration. The jump distance is then:

$$\Delta x^{(i)} = (u_2^{(i)} - u_1) / \left( \frac{du}{dx} \right)_{x=x_1} \quad (20)$$

the temperature increment is:

$$T_2^{(i)} = T_1 + \left. \frac{dT}{dx} \right|_{x=x_1} \Delta x^{(i)} \quad (21)$$

and the ionization fraction increment is:

$$\alpha_2^{(i)} = \alpha_1 + \frac{d\alpha}{dx} \Big|_{x=x_1} \Delta x^{(i)} \quad (22)$$

Equations (19) through (22) are placed in a loop where they are repeatedly evaluated until the differences in temperature and ionization fraction between two successive iterations is smaller than some specified tolerance. Thus the Mach number, velocity, temperature, and ionization fraction on the supersonic side of the sonic point are all known, along with its coordinate:

$$x_2^{(i)} = x_1 + \Delta x^{(i)} \quad (23)$$

The other properties across the sonic point are then determined using the conservation equations.

The integration of the system (15) through (18) is achieved starting from the subsonic inlet. Since not all initial conditions are known, usually a manual shooting method is used in which guessed initial estimates are refined after integration past the sonic point. Rather than relying on such an ad-hoc shooting method, an automatic algorithm for integrating the governing equations has been developed. To accomplish this, a sequence of tests have been designed which determine which inlet variable to modify and in what direction to modify it. Some of these tests are performed after a complete integration through the channel, while others are done in a specific region, such as within the jump routine. Still others are performed after every integration step. These diagnostic tests are summarized in Table I.

**Table I: Tests performed and actions taken for automatic integration of MPD channels. Variables subscripted 1 are previous points, those subscripted 2 are evaluated at the present location, and the subscript T denotes the throat, or minimum area location.**

TEST	PLACE	TRUE	FALSE
$M_2 > M_1$ ( $x < x_T$ )	every step before $x_T$	no action	restart at inlet with higher $u_o$
$M_2 > M_1$ ( $x > x_T$ )	every step after $x_T$	no action	if #successive failures > 25 restart with lower $u_o$
$T_2 > T_1$	every step before $x_T$	no action	restart with lower $u_o$
$P > 0, \alpha > 0$	every step	no action	restart with lower $u_o$
$B < 0$	every step	nozzle end; check length	no action
$ I-L  > \epsilon_L$	after completed integration	Done!	correct $E_o$ and restart
$I < L$	after completed integration	decrease $E_o$ and restart	no action
$I > L$	after completed integration	increase $E_o$ and restart	no action
$x > 1.5L$	every step	increase $E_o$ and restart	no action
$x = L$ and no jump	every step	increase $u_o$ and restart	no action

The numerical algorithm presented here has been applied to the solution of the governing equations for a constant area channel. These results have been compared to existing solutions for constant area channels[5]. The agreement is found to be good to at least the third decimal place for all the variables. In the next section, results are presented for the simplest of varying areas, i.e. linearly varying channel height.

#### IV. Results

Before discussing the varying area cases, we will briefly revisit the constant area geometry. The effect of different mass flow rates on the profiles of ionization fraction along the length of the channel is shown in Fig. 3, for mass flow rates ranging from 0.003 kg/s to 0.006 kg/s. The magnetic induction at the inlet ( $x=0$ ) is 0.159, the cross sectional area is  $0.001 \text{ m}^2$ , the length is 20 cm., and the inlet ionization fraction is 0.05. It can be seen from Fig. 3 that the density has a profound effect on the rate of ionization. From equation (7), it can be seen that the recombination term in the rate equation for  $\alpha$  varies as  $\rho^2$  in contrast to the ionization term which varies as  $\rho$ . Thus, for higher mass flow rates, and hence higher densities,  $\alpha$  actually decreases along the channel until near the exit, where the temperature increases. This effect of density on the ionization fraction has not been previously reported[5-8,12].

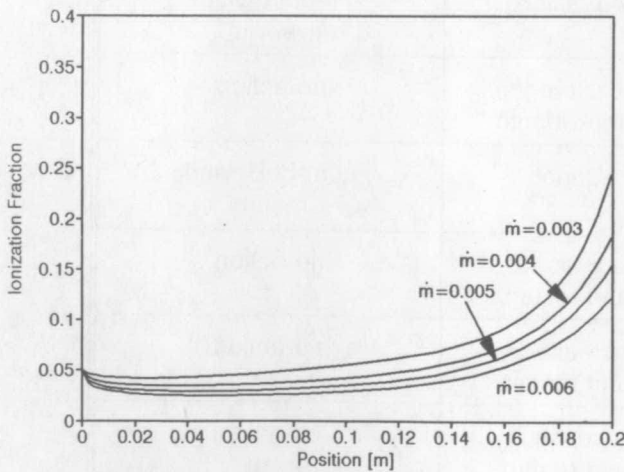


Figure 3: Ionization fraction profiles for a constant area channel,  $A = 0.001 \text{ m}^2$ ,  $B_i = 0.159$ ,  $L = 20 \text{ cm}$ , at various mass flow rates.

Let us now consider a channel with an area variation given by  $A(x) = 0.001 + x(\delta A)$ , where  $x$  is in meters and  $A(x)$  is in  $\text{m}^2$ . The total channel length is taken to be 20 cm. so that  $x \in [0.0, 0.2]$ . The four cases reported here are  $\delta A = 0$  (constant area),  $\delta A = 0.0175$ ,  $\delta A = 0.04$ , and  $\delta A = 0.07$ . The fixed quantities are inlet area  $A_i = 10 \text{ cm}^2$ , mass flow rate = 0.006 kg/s,  $B_i = 0.159$ ,  $\alpha_i = 0.05$ , and length = 20 cm. The profiles of  $u$ ,  $T$ ,  $j$ ,  $\alpha$ ,  $B$ , and  $M$  are shown in Figs. 4-9. Qualitatively, each profile is similar to those discussed previously[5]. However, the flared varying area geometry is seen to be very different in several ways when compared to the constant area geometry. First, the most obvious effect of varying area is apparent on the velocity. The exit speeds and hence specific impulses are 1.7, 2.0, and 2.2 times larger than the constant area case for area ratios of 4.5, 9, and 15 respectively. Second, the ionization fraction shows the same behavior seen in Fig. 3 for a constant area channel with the higher mass flows. The flared geometry has a dramatic effect on the ionization fraction. As the flare angle is increased, the value of  $\alpha$  is seen to increase. This is due to the aforementioned decrease in density for the same mass flow rate but different flare angles. Third, the magnetic induction shows the effects of increasing back-EMF as the flare angle is increased for a fixed mass flow rate and total current. Finally, the current density rise at the exit usually seen in the constant area channels[5] is diminished greatly by the flared geometry.

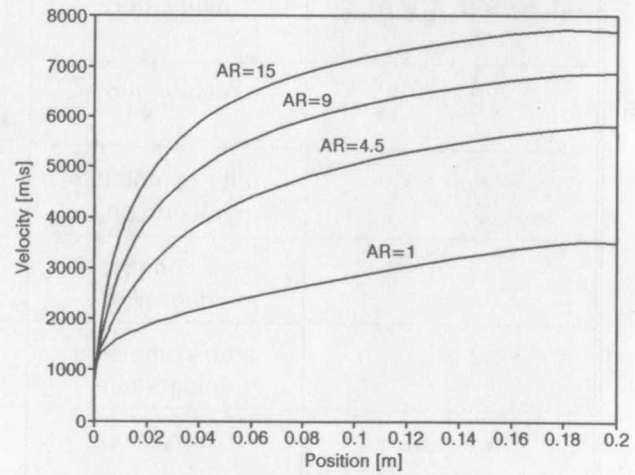
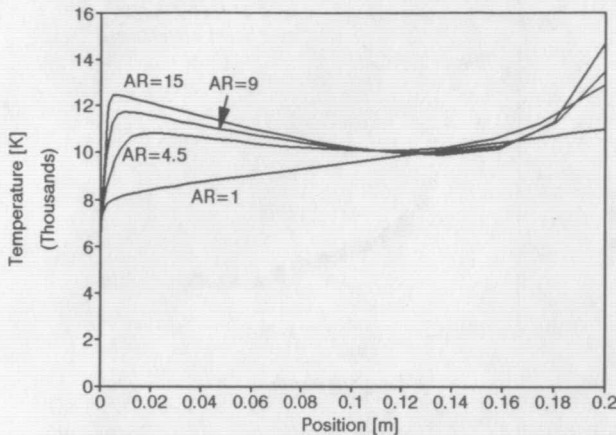
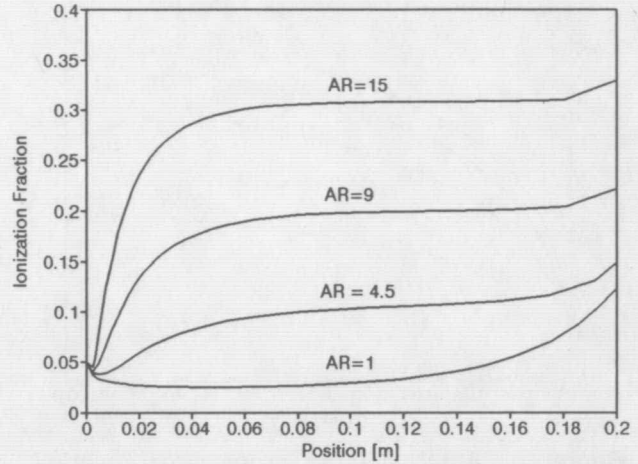


Figure 4: Velocity profiles for exit/inlet area ratios of 1 (constant area), 4.5, 9, and 15, with  $A_i = 0.001 \text{ m}^2$  and 20 cm. length.



**Figure 5:** Temperature profiles for linearly-varying areas,  $A_i = 0.001 \text{ m}^2$  and 20 cm. length.



**Figure 7:** Ionization fraction profiles for linearly-varying areas,  $A_i = 0.001 \text{ m}^2$  and 20 cm. length.

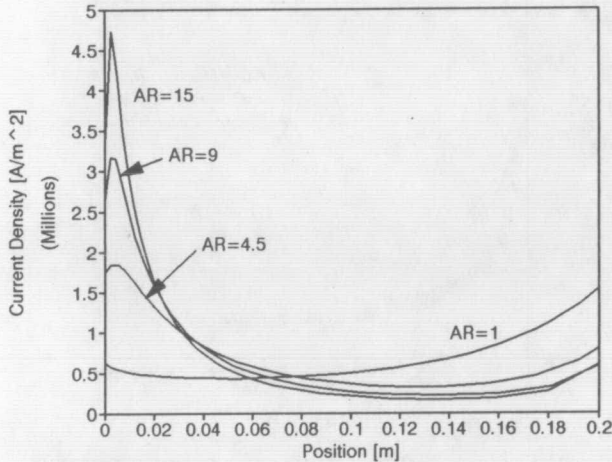


**Figure 6:** Current density profiles for linearly-varying areas,  $A_i = 0.001 \text{ m}^2$  and 20 cm. length.

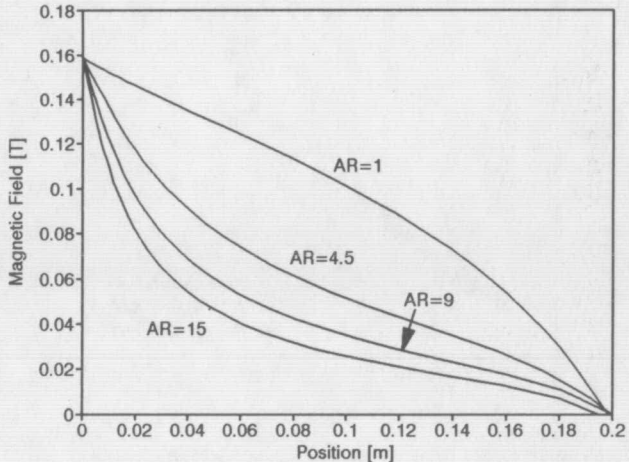


**Figure 8:** Magnetic field profiles for linearly-varying areas,  $A_i = 0.001 \text{ m}^2$  and 20 cm. length.

We now turn our attention to a modified version of the original King anode[17]. Thrust measurements have recently been made on the Half-Scale Flared Anode Thruster (HSFAT)[18]. Comparisons between these HSFAT measurements and two-dimensional axisymmetric frozen, fully ionized flow modelling results have also recently been performed[19]. The HSFAT is essentially the same shape as the original King anode[17], but much shorter in axial length (10 cm. versus 20 cm.). Figures 10 through 12 show comparisons of thrust and thrust-to-total current squared, between the present quasi one-dimensional model, experimental measurements, and the numerical

results of LaPointe[19]. As can be seen, the agreement is excellent. Furthermore, there is a subtle inflection point around 11 kA in the experimental results shown in Fig. 10 that is correctly reproduced in the present results. Also, there is a dramatic increase in thrust beyond approximately 21 kA. The present quasi one-dimensional predictions end around 16 kA because the flow is nearly fully ionized over a significant length inside the thruster (see Fig. 13). We conclude therefore that the dramatic increase in thrust at currents above 20 kA is due to the presence of doubly charged ions, which we have not considered here. It is also interesting to note the typical current density and back-EMF profiles

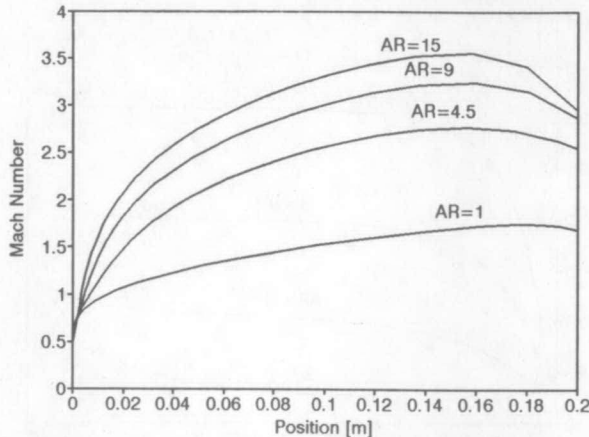


**Figure 9:** Mach number profiles for linearly-varying areas,  $A_i = 0.001 \text{ m}^2$  and 20 cm. length.

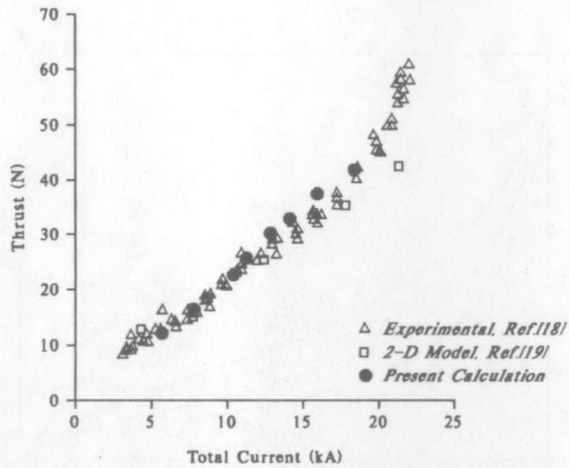


**Figure 10:** Comparison of experimentally measured and calculated values of thrust for 10 cm. HSFAT channel.

shown in Figs. 14 and 15. Also plotted in these figures for reference are the corresponding curves for a linear flared anode (i.e. area varying continuously from inlet to exit). The back-EMF is highest in the region where the electric field is highest, and lower where the electric field is lower. This is in contrast to the straight coaxial thruster where the electric field is constant and the back-EMF reaches a maximum in the region approximately midway between inlet and exit. Such nozzle contouring can therefore help control Onset due to an excessive back-EMF[4,5].

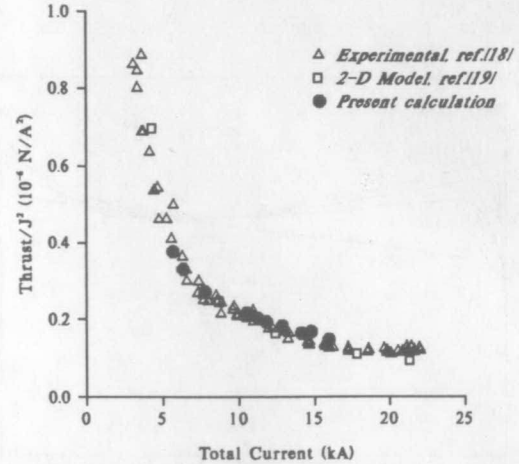


**Figure 11:** Comparison of experimentally measured and calculated values of thrust/ $J^2$  for 10 cm. HSFAT channel.

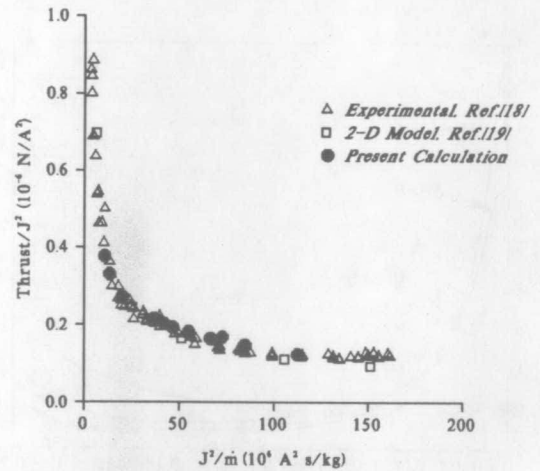


**Figure 12:** Comparison of experimentally measured and calculated values of thrust/ $J^2$  for 10 cm. HSFAT channel.

## V. Summary & Conclusions

An efficient algorithm utilizing the Bulirsch-Stoer method for integration of quasi one-dimensional ionizing MPD flow has been presented. Solutions have been compared with previous solutions for constant area channels, and have revealed features not reported in previous studies[5-8,12]. This work has revealed that for a fixed geometry (constant area channel) and total current, the exit ionization fraction increases with decreasing mass flow rate. Furthermore, for a fixed mass flow rate and total current, substantial increases in ionization fraction and specific impulse may be

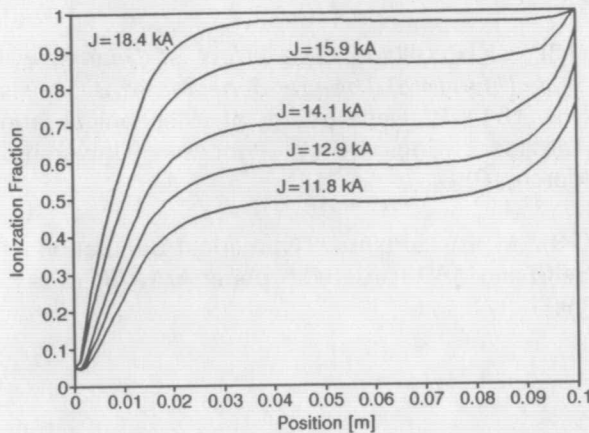


**Figure 13:** Comparison of ionization fraction profiles in 10 cm. HSFAT channel.

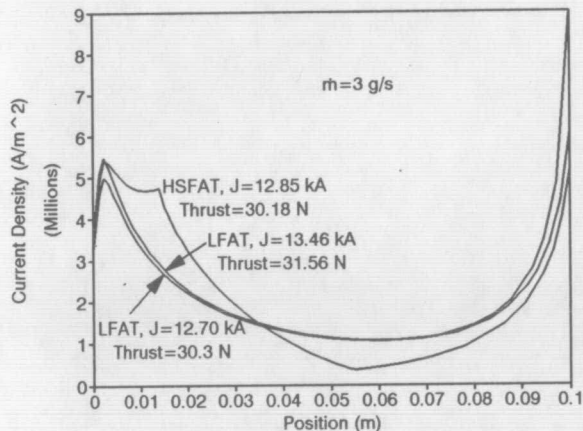


**Figure 14:** Comparison of HSFAT current density profile with that of a linearly-varying channel with the same  $A$ , and  $A_e$ .

achieved by using a flared geometry. Too much of a flare or abrupt expansion, however, can lead to Onset by the back-EMF mechanism[5]. Comparison of the present model with measurements on the HSFAT show excellent agreement. This suggests that thruster geometries can be optimized for specific operating points (i.e. total current and mass flow rate) to maximize thrust and specific impulse, using the present model.

#### Acknowledgements

The authors acknowledge helpful discussions with Dr. J. L. Lawless, Space Power, Inc. This work was supported by AFOSR-87-0360.

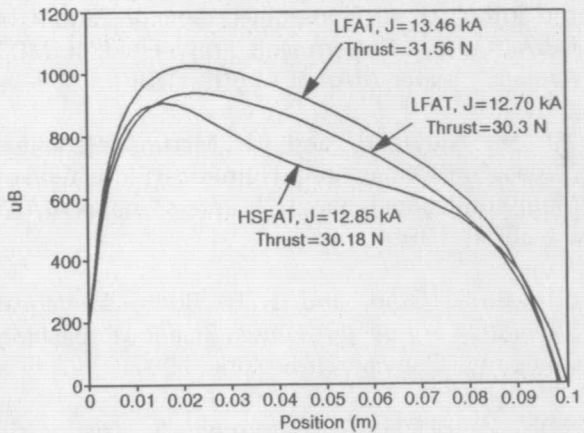


**Figure 15:** Comparison of back-EMF of HSFAT with that of a linearly-varying channel with the same  $A$ , and  $A_e$ .

#### References

- (1) R. K. Seals, and H. A. Hassan, "Analysis of MPD Arcs with Nonequilibrium Ionization", *AIAA J.*, Vol. 6, pp. 2273-2278, December 1968.
- (2) F. G. Baksht, B. Ya. Moizhes, and A. B. Rybakov, "Critical Regime of a Plasma Accelerator", *Sov. phys.-Tech. Phys.*, Vol. 18, No. 12, pp 1613-1616.
- (3) D. O. King, K. E. Clark, and R. G. Jahn, "Effect of Choked Flow on Terminal Characteristics of MPD Thrusters", paper AIAA-81-0686, 1981.
- (4) J. L. Lawless, and V. V. Subramaniam, "Theory of Onset in Magnetoplasmadynamic Thrusters", *J. Propulsion & Power*, Vol. 3, pp. 121-127, March-April 1987.
- (5) V. V. Subramaniam, and J. L. Lawless, "Onset in Magnetoplasmadynamic Thrusters with Finite Rate Ionization", *J. Propulsion & Power*, Vol. 4, No. 6, pp. 526-532, November-December 1988.
- (6) M. Martinez-Sanchez, "Structure of Self-Field Accelerated Plasma Flows", *J. Propulsion & Power*, Vol. 7 (1), pp. 56-64, Jan.-Feb. 1991.

- (7) T. Shoji, and I. Kimura, "Analytical Study on the Influence of Non-equilibrium Ionization for Current Flow Pattern and Flow Field of MPD Arcjets", paper AIAA-90-2609, 1990.
- (8) E. Niewood, and M. Martinez-Sanchez, "Quasi One-Dimensional Numerical Simulation of Magnetoplasmadynamic Thrusters", paper AIAA-90-2604, 1990.
- (9) E. S. Oran, and J. R. Boris, *Numerical Simulation of Reactive Flows*, Science Publishing Company, Elsevier, New York, 1987.
- (10) Z. Bilicki, C. Dafermos, J. Kestin, G. Majda, and D. L. Zeng, "Trajectories and Singular Points in Steady State Models of Two-Phase Flows", *Int. J. Multiphase Flow*, Vol. 13, No. 4, pp. 511-533, 1987.
- (11) V. V. Subramaniam, and J. L. Lawless, "Electrode -Adjacent Boundary Layer Flow in Magnetoplasmadynamic Thrusters", *Phys. Fluids* 31 (1), pp. 201-209, January 1988.
- (12) M. Martinez-Sanchez, "The Structure of Self-Field Accelerated Plasma Flows", paper AIAA-87-1065, May 1987.
- (13) K. Kuriki, and T. Nakayama, "Magnetosonic Condition in Magnetoplasmadynamic Flow", paper AIAA-87-1065, May 1987.
- (14) C. W. Gear, "The Automatic Integration of Ordinary Differential Equations", *Numerical Mathematics, Communications of the ACM*, Vol. 14, No. 3, March 1991.
- (15) R. Bulirsch, and J. Stoer, "Numerical Treatment of Ordinary Differential Equations by Extrapolation Methods", *Numerische Mathematik*, Vol. 8, pp. 1-13, 1966.
- (16) Glenn Lefever-Button, "Quasi One-Dimensional Ionizing Supersonic Flow in a Magnetoplasmadynamic Thruster", *Undergraduate Honors Thesis*, College of Engineering, The Ohio State University, July 1990.
- (17) D. Q. King, *Magnetoplasmadynamic Channel Flow for Design of Coaxial MPD Thrusters*, Ph.D. Dissertation, Princeton University, December 1981.
- (18) J. H. Gilland, *The Effect of Geometrical Scale Upon MPD Thruster Behavior*, M.S. Thesis No. 1811-T, Department of Mechanical and Aerospace Engineering, Princeton University, March 1988.
- (19) M. R. LaPointe, "Numerical Simulation of Self-Field MPD Thrusters", paper AIAA-91-2341, 1991.